

# Chapter 2

## *Experimental*

### **2.1 Introduction**

This Chapter gives an overview of the materials, methods and characterisation techniques used within this study. It is divided into three sections which describe:

- materials used consistently throughout this work. Included is the rationale behind the selection of specific rolling oils and rolling oil ingredients for analysis;
- techniques used in the preparation of samples, and
- methods used to characterise sample properties.

Details of materials, sample preparation techniques and characterisation methods pertaining to particular aspects of this work are detailed in the relevant chapters.

### **2.2 Materials**

#### **2.2.1 Selection of Commercial Cold Rolling Oil Formulations**

The twelve commercial cold rolling oil formulations studied in this work, denoted XR81627, XR81628, XR81629, BSLWP1.1, 560453, 560350, 560350noS, U1388501, SB4198, CAT29, N609DPD and XR82154, were supplied by Quaker Chemical (Australasia) and prepared according to the method described in section 2.3.1.1. The formulations are complex blends of up to thirteen different ingredients including base esters, lubrication additives, viscosity modifying agents, emulsifiers, antioxidants and corrosion inhibitors and were selected to cover a broad range of oils used in different types of cold rolling mills around the world and to include oils which industrial observations have shown to give rise to both good and poor hot dip metallic coating quality.<sup>1</sup> The generic compositions of the oils with respect to key rolling oil ingredients (described in more detail in section 2.2.2 and in the relevant chapters), together with the oil physical properties where available (saponification value and viscosity) are provided in table 2.1.

Table 2.1 Generic compositions and physical properties of the twelve commercial cold rolling oils used in this study.

Ingredient	Concentration Range (% w/w)	Rolling Oil Formulation											
		XR81627	BSLWP1.1	560453	560350noS	U1388501	SB4198	CAT29	N609DPD	560350	XR82154	XR81628	XR81629
<i>tallow</i>	30-100												
<i>ester A (semi-synthetic)</i>	44-64												
<i>ester B (fully-synthetic)</i>	28-30												
<i>ester C (semi-synthetic)</i>	29												
<i>coconut oil</i>	18-30												
<i>phosphate ester</i>	0.19-0.40												
<i>amine phosphate</i>	0.30-0.60												
<i>sulfurised lard oil (SLO)</i>	6.0-20												
<i>sulfurised vegetable oil (SVO)</i>	3.0												
<i>di-tert-dodecyl trisulfide (TPS20)</i>	1.5												
<b>Properties*</b>													
<i>viscosity (cSt @ 40 °C)</i>		-	42	55	-	55	52	-	53	47	-	-	-
<i>saponification value (mg KOH g<sup>-1</sup>)</i>		-	177	160	-	210	205	-	163	160	-	-	-

\* Courtesy of Quaker Chemical (Australasia).

### 2.2.2 Selection of Rolling Oil Ingredients

Research has shown that oil-derived residues remaining on the surface of cold rolled steel following the continuous annealing process can give rise to the formation of uncoated defects in hot dip metallic coatings.<sup>2-11</sup> Rolling oils (and rolling oil ingredients) which thermally decompose to form significant amounts of residue are therefore more likely to impact detrimentally upon hot dip metallic coating quality than oils which decompose cleanly. In order to select rolling oil ingredients for analysis in the present study, screening tests were performed by Thermogravimetric Analysis (TGA). Seventeen different commonly used ingredients, supplied by Quaker Chemical (Australasia) and whose use is described in table 2.2, were thermo-oxidatively decomposed using the procedure described in section 2.4.1. The amount of residue remaining at 500 °C (the average maximum steel surface temperature employed during the continuous annealing process) was measured for each ingredient and normalised against the maximum ingredient concentration according to equation 2.1:

$$NR = \frac{R}{100} \times C \quad \text{Equation 2.1}$$

where NR is the normalised % residue at 500 °C, R is the % residue at 500 °C and C is the typical maximum ingredient concentration employed in commercial cold rolling oil formulations. Table 2.1 summarises the results obtained.

Base esters, the corrosion inhibitor and lubrication additives thermo-oxidatively decompose to leave the greatest amounts of thermally-stable residue at 500 °C. However, the normalised % residue values indicate that base esters A and B, coconut oil, sulfurised lard oil (SLO), sulfurised vegetable oil (SVO) and the phosphate ester are more likely to contribute to high residue levels in fully-formulated cold rolling oils and that the corrosion inhibitor, dimer acid and amine phosphate ingredients typically constitute such a minor fraction of an oil formulation that their residue contribution is minimal. The identification of these ingredients as being potentially problematic to hot dip metallic coating quality is in accordance with observations made by industry;

commercial rolling oils containing SLO and SVO often give rise to uncoated defects.<sup>1</sup>

Given this, the following oil ingredients were selected for further investigation:

- base esters A, B and C and coconut oil;
- sulfurised lubrication additives (dialkyl pentasulfide (DAPS), di-*tert*-dodecyl trisulfide (TPS 20), SLO and SVO), and
- phosphorus-based lubrication additives (amine phosphate and phosphate ester).

Ingredients which leave lesser amounts of residue (ester C, DAPS, TPS 20 and the amine phosphate) have been included in the above selection for comparative purposes.

The chemical structures of these ingredients are described in the relevant chapters.

**Table 2.2 Summary of the properties, % residue at 500 °C and normalised % residue at 500 °C values determined for seventeen cold rolling oil ingredients by TGA. Errors are less than  $\pm 20$  %.**

<b>Ingredient</b>	<b>Function</b>	<b>Max. Ingredient Concentration in Formulation (% w/w)</b>	<b>% Residue at 500 °C</b>	<b>Normalised % Residue at 500 °C</b>
ester A	Base Stock	90	0.36	0.32
ester B		30	2.8	0.84
ester C		90	0	0
polyolefin		5	0	0
coconut oil		30	1.7	0.52
emulsifier A	Miscellaneous Additives	5	0	0
emulsifier B		5	0	0
metal deactivator		1	0.02	0
antioxidant		1	0.95	0.01
corrosion inhibitor		0.5	28	0.14
DAPS	Lubrication Additives	5	1.7	0.09
TPS 20		5	2.1	0.11
SLO		10	11	1.1
SVO		10	6.8	0.68
dimer acid		3	4.3	0.13
phosphate ester		2	11	0.23
amine phosphate		1	13	0.13

### 2.2.3 Steel

Cold rolled low-carbon steel, supplied by BlueScope Steel<sup>®</sup> and whose physical and chemical properties are given in table 2.2, was used throughout this work.

**Table 2.3 Properties of the low-carbon steel used. Analysis by Atomic Emission Spectroscopy courtesy of BlueScope Steel<sup>®</sup>'s Central Laboratory.**

<b>Chemical Properties</b>	
<b>Element</b>	<b>Nominal Percentage</b>
Iron	~ 99.7
Carbon	0.050
Phosphorus	0.014
Manganese	0.20
Silicon	0.005
Sulfur	0.014
Nickel	0.028
Chromium	0.018
Molybdenum	<0.002
Copper	0.021
Aluminium	0.036
Tin	<0.002
Niobium	<0.001
Titanium	<0.003
Vanadium	<0.003
Boron	<0.0003
Calcium	<0.0005
Nitrogen	0.0032
<b>Physical Properties</b>	
<b>Thickness</b>	0.42 mm
<b>Yield Strength (MPa)</b>	550

### 2.2.4 55Al-43.4Zn-1.6Si Hot Dip Metallic Coating Alloy

Zincalume<sup>®</sup> (55Al-43.4Zn-1.6Si) hot dip metallic coating alloy, supplied by BlueScope

Steel<sup>®</sup>, was used in all hot dip simulation and industrial hot dipping trial experiments. The chemical properties of this alloy are given in table 2.3.

**Table 2.4 Properties of the 55Al-43.4Zn-1.6Si hot dip metallic coating alloy used. Analysis by Atomic Emission Spectroscopy courtesy of BlueScope Steel<sup>®</sup>'s Central Laboratory.**

<b>Element</b>	<b>Nominal Percentage</b>
Aluminium	55.2
Zinc	42.6
Silicon	1.5
Iron	0.44
Titanium	<0.005
Calcium	0.02
Vanadium	0.005
Chromium	<0.005
Zirconium	<0.005
Boron	<0.005

### **2.2.5 Solvents and Other Chemicals**

The Shellite (a paraffinic/naphtha-based distillate) and ethanol solvents used to clean cold rolled steel samples prior to hot dip simulation experiments were provided by BlueScope Steel<sup>®</sup>'s Research Laboratories. Reagent grade lithium tetraborate powder and nitric acid, used in the cleaning of platinum TGA pans, and acetone and ethanol, used to degrease cold rolled steel samples for confocal microscopy experiments, were purchased from Sigma-Aldrich Australia.

### **2.2.6 Gases**

The oxygen, 5 % hydrogen-95 % nitrogen (HNX), nitrogen and argon gases used in this study were all of high purity and were supplied by BOC Gases Australia.

### **2.2.7 Thermal Analysis Consumables**

The platinum crucibles used to suspend samples in TGA experiments and the standard

aluminium pans used to hold oil samples in both TGA and Pressure Differential Scanning Calorimetry (PDSC) experiments were sourced from TA Instruments. The aluminium pans were passed through a Bunsen burner flame to volatilise contaminants prior to use and the platinum crucibles were cleaned by filling with lithium tetraborate powder, heating to 1000 °C, cooling to room temperature and finally warming in 10 % nitric acid solution to remove excess lithium salt. The choice of aluminium pans, as opposed to steel pans (used by Zhang et al.<sup>12, 13</sup> in their PDSC 2-peak test), steel puck inserts (used by Quaker Chemical in their variation of Zhang's PDSC 2-peak test<sup>14</sup>) or oil/iron oxide powder blends (used by Sech et al.<sup>2</sup> for rolling oil analysis under HNX), in TGA and PDSC experiments was based upon multiple considerations. With respect to PDSC analysis, steel DSC pans/steel puck inserts in aluminium pans/iron oxide powder were not used due to:

- the contribution of iron oxide powder/steel oxidation to heat flow;
- steel puck stress relaxation disrupting contact with the sample platform;
- difficulties in ensuring good thermal contact between the steel puck/aluminium pan assembly and the sample platform (the steel puck was often concave in shape);
- frequent oil leakage over the steel puck edges, and
- difficulties in ensuring consistent sampling of oil/iron oxide powder blends.

The above factors all give rise to variations in the oil decomposition mechanism and therefore cause problems with test reproducibility and increase experimental error margins. This is supported by the findings of Sharma et al.,<sup>15</sup> who noted that flat-bottom aluminium pans produce a lower standard deviation for PDSC analysis of lubricating oils than alternatives such as solid fat index pans or hermetic pans. Additional advantages of using aluminium pans are that they are cheap, commercially produced (and therefore of consistent metallurgical composition), readily available, they provide a mild catalytic effect on oil oxidation<sup>16</sup> and they produce an oil decomposition profile analogous to that observed by use of steel puck and iron oxide powder (refer to Chapter 5). The advantage of using aluminium pans for TGA analysis is they do not contribute significantly to % residue measurements under highly oxidising conditions.

Consequently, standard aluminium pans were used in all PDSC and the majority of TGA analyses (unless otherwise stipulated) to ensure the comparability of results obtained using different technique and to minimise experimental error. Lids were not used in PDSC experiments to optimise oil exposure to the surrounding oxygen atmosphere.

## **2.3 Sample Preparation Techniques**

### **2.3.1 Oil Blends**

Two types of oil samples were analysed in this work; fully-formulated commercial cold rolling oils and model blends of single oil ingredients in a generic base ester. The preparation of each of these types of oils is described below.

#### **2.3.1.1 Cold Rolling Oil Formulations**

Commercial cold rolling oils XR81627, XR81628, XR81629, BSLWP1.1, 560453, 560350, 560350noS, U1388501, SB4198, CAT29, N609DPD and XR82154, whose compositions with respect to key ingredients are provided in table 2.1 (the exact compositions of these formulations are confidential), were formulated gravimetrically by weighing constituents into a tared beaker. The beaker contents were stirred on a hotplate at 60 °C until dissolution of all ingredients was complete (minimum 5 mins) and an homogeneous mixture was obtained. All rolling oil samples were warmed to 60 °C and shaken to ensure homogeneity prior to sampling for analysis by TGA, PDSC or hot dipping.

#### **2.3.1.2 Model Base Ester/Additive Blends**

Single-component blends of key oil additives (SLO, SVO, TPS 20, DAPS, phosphate ester and amine phosphate) were prepared in base ester A, an ubiquitous commercial cold rolling base ester (refer to section 3.2.2.1.1 in Chapter 3 for a description of ester A's chemical structure) to achieve a variety of different sulfur (SLO, SVO, TPS 20, DAPS) or phosphorus (phosphate ester, amine phosphate) concentrations spanning the range used in commercial cold rolling oil formulations. Descriptions of the formulation

properties of these blends are provided in the relevant chapters. A total of 2.5 g of each mixture was prepared to minimise errors due to variations in ingredient mass between blends. The additive/ester A blends were formulated gravimetrically by weighing constituents into a tared glass vial. The resultant mixture was then stirred on a hotplate at 60 °C for a minimum of 5 mins until an homogeneous mixture was obtained. All additive/ester A blend samples were warmed to 60 °C and shaken to ensure homogeneity prior to sampling for analysis by TGA, PDSC or hot dipping.

### **2.3.2 Attenuated Total Reflectance Spectroscopy (ATR)**

Infrared spectroscopy is an analytical technique which examines the interaction between a material and electromagnetic radiation in either the near (13000-4000  $\text{cm}^{-1}$ ), mid (4000-400  $\text{cm}^{-1}$ ) or far (400-40  $\text{cm}^{-1}$ ) infrared regions where molecular vibrational and rotational bands are observed.<sup>17</sup> Chemical functional groups absorb infrared radiation of characteristic frequencies so that infrared analysis can be used to detect the presence (and concentration) of different chemical moieties present in the sample.<sup>17</sup> Many different surface-sensitive infrared spectroscopic sampling configurations are available, including Diffuse Reflectance (DRIFT), Photoacoustic FTIR (PAS), grazing angle Infrared Reflection-Absorption (IRRAS) and Attenuated Total Reflectance (ATR). The selection of the appropriate technique is highly dependent upon the geometrical and physical properties of the material for analysis.<sup>18</sup>

ATR has been used extensively for the qualitative analysis of films and coatings in the sub- to several micrometre thickness range.<sup>18-20</sup> In this technique, the sample is placed into intimate contact with the surface of the ATR crystal (also known as an internal reflection element), a hard, optically transparent material with a high refractive index. The principle of ATR relies on the different refractive indices of the ATR crystal and the sample to cause a distortion in the path of the infrared radiation as it passes from one medium the other.<sup>19</sup> The majority of radiation is transmitted at an angle of incidence,  $\theta$ , of 90 °. However, if the angle of incidence is greater than the critical angle,  $\theta_c$ , which is proportional to the refractive indices of the crystal and sample, then total internal

reflection will occur at the crystal/sample interface.<sup>19</sup>

According to Maxwell's theory, when light propagates through an optically thin, non-absorbing medium an evanescent wave perpendicular to a totally reflecting surface is generated (figure 2.1).

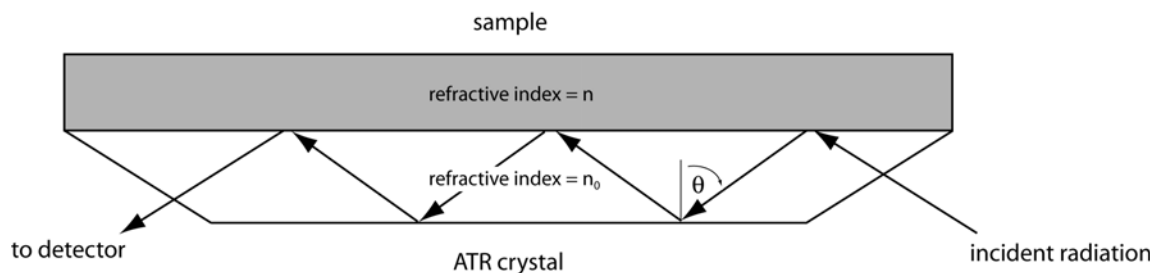


**Figure 2.1** Schematic diagram showing multiple reflections of incident infrared radiation at the sample/ATR crystal interface.

The depth to which this wave can penetrate into the sample ( $d_p$ ) depends on  $\theta$ , the refractive index difference between the ATR crystal and the sample and the frequency of the incident radiation (equation 2.2):<sup>19, 20</sup>

$$d_p = \frac{\lambda}{2\pi(n_0^2 \sin^2 \theta - n^2)^{1/2}} \quad \text{Equation 2.2}$$

where  $n_0$  and  $n$  are the refractive indices of the ATR crystal and the sample respectively and  $\lambda$  is the radiation wavelength.

If the sample absorbs some of the penetrating radiation then the infrared beam is attenuated and measured by the spectrophotometer as a function of wavelength to produce an infrared spectrum. The absorption of radiation at multiple reflection points along the crystal/sample interface increases the sensitivity of the ATR technique. Correction for the variation of sampling depth as a function of wavenumber can then be achieved through the application of an appropriate algorithm.<sup>19</sup>

ATR was selected as the appropriate method for infrared analysis in the present study

due to its availability, surface sensitivity, non-specific sample geometry requirements and the fact that it can be used to rapidly acquire sample spectra without the need for lengthy preparations such as grinding or gas purging.

Room temperature samples were prepared for ATR analysis by weighing  $1.0 \pm 0.2$  mg of the desired rolling oil ingredient into a standard aluminium pan. The pan sides were then cut using a scalpel, enabling it to be flattened out for ATR analysis (figure 2.2).

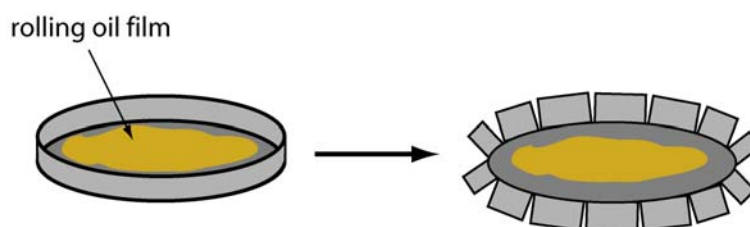


**Figure 2.2 Preparation of rolling oil samples for ATR analysis.**

Thermally decomposed oil samples were prepared for ATR analysis by TGA as opposed to PDSC to enable rapid analysis following sample decomposition, thereby minimising the occurrence of chemical changes in the sample between preparation and analysis. The time lapse between sample preparation and ATR analysis was approximately two minutes and it was found that leaving the samples for any length of time resulted in further volatilisation and chemical changes. Given that PDSC samples would have to be cooled to below  $100\text{ }^{\circ}\text{C}$  before removal of the sample from the pressure cell, the PDSC technique was deemed to be unsuitable for sample preparation for ATR analysis. The thermally decomposed samples were prepared by heating to a series of temperatures ranging from  $100\text{--}500\text{ }^{\circ}\text{C}$  (samples were typically prepared at  $100\text{ }^{\circ}\text{C}$ ,  $150\text{ }^{\circ}\text{C}$ ,  $200\text{ }^{\circ}\text{C}$ ,  $250\text{ }^{\circ}\text{C}$ ,  $300\text{ }^{\circ}\text{C}$ ,  $350\text{ }^{\circ}\text{C}$ ,  $400\text{ }^{\circ}\text{C}$ ,  $450\text{ }^{\circ}\text{C}$  and  $500\text{ }^{\circ}\text{C}$ ; other temperatures were used when complex chemical changes were taking place over narrow temperature ranges) using the TGA procedure described below. Fresh quantities of material were used in the creation of each sample. Following TGA treatment, the aluminium pan was flattened out for ATR analysis as described above. Analyses were performed in duplicate to confirm reproducibility.

### 2.3.3 Hot Dip Simulation Experiments

Hot dip simulation experiments were conducted at BlueScope Steel<sup>®</sup>'s Research Laboratories using the purpose-built apparatus shown in figure 2.3.

The apparatus comprises of:

- a pneumatically-driven dipping arm from which a steel sample is suspended;
- an infrared furnace to preheat the sample under a controlled atmosphere prior to dipping;
- a slide gate valve to separate the preheat furnace from the dipping chamber;
- an isolated dipping chamber kept at constant temperature under an 5 % hydrogen-95 % nitrogen (HNX) atmosphere to prevent oxidation of the molten alloy coating;
- a crucible containing the molten alloy coating, and
- a melt furnace used to heat and maintain the molten alloy at a constant temperature.

Cold rolled steel samples were cut to 100 mm x 30 mm to fit within the diameter of the crucible whilst ensuring adequate sample length for immersion into the molten alloy. Residual cold rolling oil was removed from the sample surface using the standard procedure developed by BlueScope Steel<sup>®</sup>, involving wiping the sample surface with a cloth soaked in Shellite, followed by wiping with cloth soaked in ethanol. The samples were not pickled in hydrochloric acid solution due to their large size and the need to maintain a uniform surface oxide layer.

A type-K thermocouple was spot-welded onto the sample surface to record temperature and control the heating feedback loop. A thin film of oil was then wiped onto both sides of the sample surface using a cotton bud applicator and the sample was suspended from the bottom of the simulation apparatus dipping arm.

In the first stage of the dipping cycle the sample was moved into the infrared furnace purged with nitrogen at a flow rate of 10 L min<sup>-1</sup>. Following a soaking time of 180 s, the gas was switched to HNX and the chamber was purged at 10 L min<sup>-1</sup> for a further 180 s to establish a reducing environment. The sample was then heated at 100 °C min<sup>-1</sup> to 500 °C and held isothermally for 300 s to preheat the steel and thermo-reductively decompose the rolling oil film.

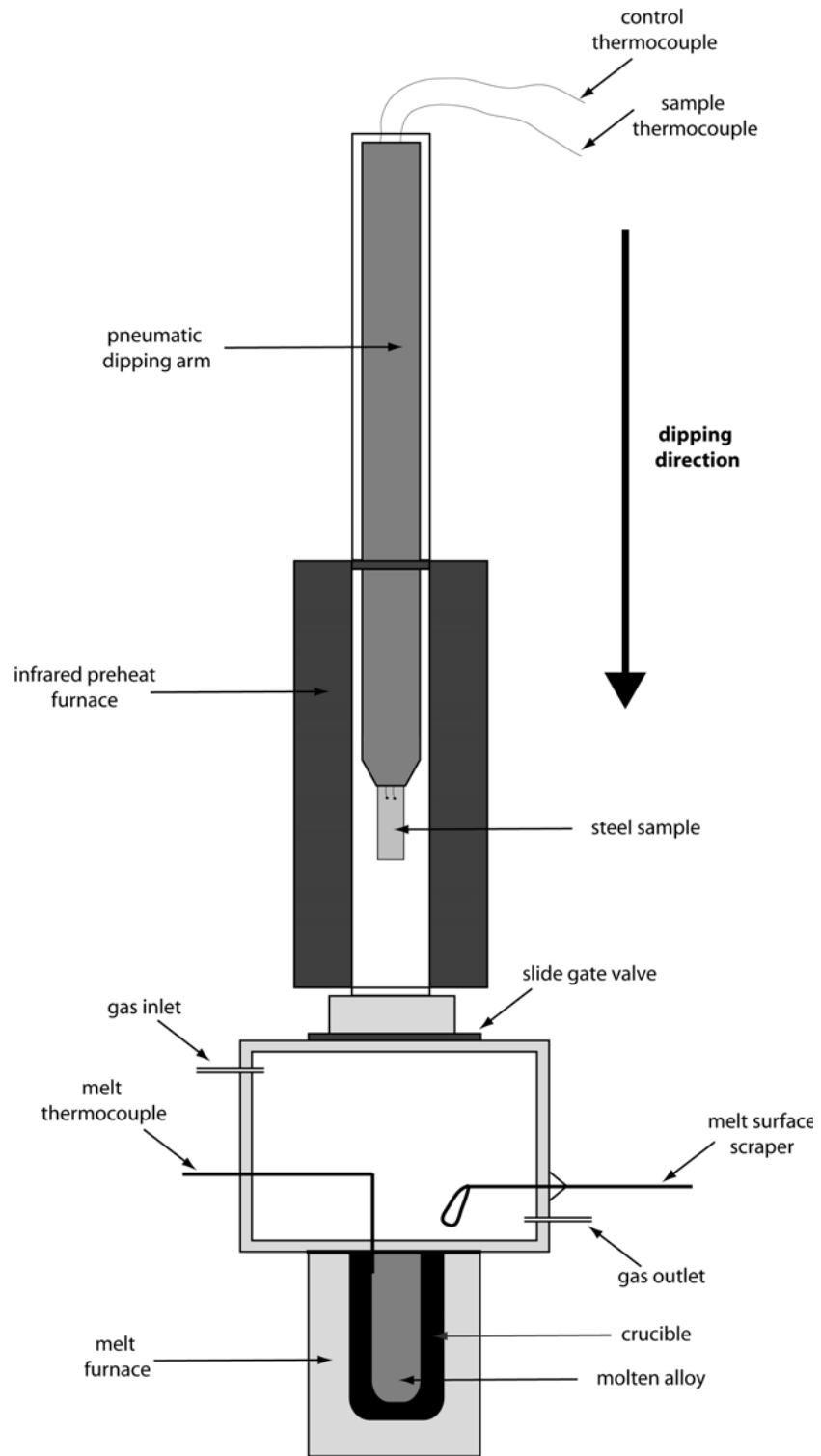


Figure 2.3 Schematic representation of the hot dip simulation apparatus.

The preheat temperature was chosen to mimic the average maximum steel surface temperature reached in the industrial continuous annealing process and the isothermal holding time was selected to ensure complete volatilisation of the rolling oil film as well as adequate reduction of steel surface oxides. Dross accumulated on the coating bath surface was removed using a scraper immediately before the dipping process commenced, ensuring a fresh melt surface. During dipping, the sample was lowered into the alloy coating bath, which was maintained under an HNX atmosphere at a temperature of 600 °C. An immersion time of 3 s was chosen on the basis of the work of Williams.<sup>21</sup> The sample was then removed from the coating bath at a rate of 1 m s<sup>-1</sup> and cooled rapidly under a stream of air to solidify the alloy coating. Experiments were performed in duplicate and control samples consisted of steel cleaned with Shellite and acetone.

Unfortunately it was not possible thermo-oxidatively decompose the rolling oil film due to the requirement for adequate, uniform reduction of steel surface oxides. However, the coating results obtained are in good agreement with industrial hot dipping trial observations such that hot dip simulation experiments are a useful tool for gauging rolling oil performance with respect to metallic coating quality.

#### **2.3.4 Industrial Hot Dipping Trials**

Assistance in carrying out the industrial-scale hot dipping trials was provided by Mr Kevin Podolski (BlueScope Steel<sup>®</sup>), Mr Andrew Gibson (Quaker Chemical Australasia), Ms Bridget Newman (BlueScope Steel<sup>®</sup>) and Mr Warren Bell (BlueScope Steel<sup>®</sup>). Access to the cold rolled steel strip was gained at the beginning of BlueScope Steel<sup>®</sup>'s metal coating line 3 (MCL3) at Port Kembla within the section where the strip is welded to the preceding coil of steel (refer to figure 1.3 in Chapter 1). Preparation of the samples close to the area where the steel is welded aided in sample recognition following the hot dipping process.

Residual rolling oil was quickly wiped from the cold rolled steel surface using a cloth soaked in Shellite. Further cleaning was not employed due to the limited timeframe

available for sample preparation. The sample area was then outlined by tracing around a 100 mm x 200 mm steel template with a black marker pen; failure of the alloy coating to adhere to this outline simplified sample recognition following the hot dipping process. Approximately 6 g of rolling oil was then poured onto the steel surface within the outlined area and spread to create a thin, even oil film. The samples were then coated in MCL3 and retrieved where the strip is cut after re-coiling.

Control samples consisted of uncleaned steel (i.e. an outlined area of the surface where the original rolling oil film was intact), Shellite-cleaned steel and Shellite-cleaned steel with a thin film of the Port Kembla rolling oil re-applied to the surface.

## 2.4 Characterisation Techniques

### 2.4.1 Thermogravimetric Analysis (TGA)

TGA is based upon the accurate measurement of changes in the mass of a sample as a function of temperature and/or time.<sup>22</sup> The TGA furnace assembly employed in the current research is shown in figure 2.4.<sup>22</sup>

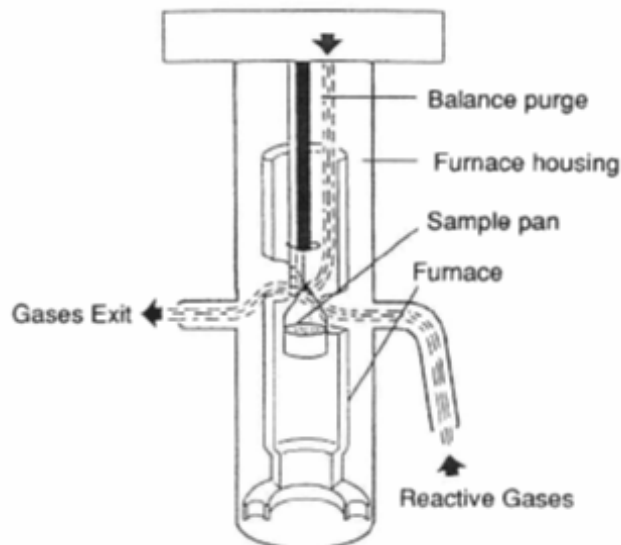


Figure 2.4 Schematic diagram of a TGA furnace assembly.<sup>22</sup>

The sample is placed into a tared pan which is suspended from a sensitive microbalance and enclosed in a furnace. The furnace and balance are then purged with the desired gas at a user-defined flow rate and the furnace is heated according to a controlled programme comprising of, for example, constant temperature ramps and/or isothermal periods. A quantitative plot of the mass and/or mass change (y axis) versus temperature or time (x axis) is obtained.

A variation of the conventional TGA technique is Modulated Thermogravimetric Analysis (MTGA).<sup>23-25</sup> MTGA overcomes many of the drawbacks associated with kinetic analysis by conventional TGA experiments; assumptions of the reaction kinetics are not required and kinetic parameters can be determined from a single experiment. This is achieved by imposing a sinusoidal temperature modulation upon the sample in addition to the linear heating profile used in conventional TGA. An oscillatory response in the rate of sample mass loss is obtained and this signal can be deconvoluted via a real-time discrete Fourier transform to yield kinetic parameters such as activation energy as a function of time, temperature or sample conversion on a continuous, 'model-free' basis. The equation used to calculate kinetic parameters by MTGA is described in Chapter 5.

In the present study, a TGA 2950 Thermogravimetric Analyzer (TA Instruments) was used for all TGA and MTGA analyses (this section only describes the conditions used for conventional TGA experiments; the conditions used for MTGA experiments are discussed in Chapter 5). The instrumental temperature calibration was performed using the Curie temperatures of nickel and alumel standard reference materials (TA Instruments). Rolling oil/oil ingredient samples were analysed in triplicate under continuous heating conditions between room temperature and 600 °C. Unless otherwise stipulated, a heating rate of 10 °C min<sup>-1</sup> and a gas flow rate of 50 ml min<sup>-1</sup> were employed. High purity oxygen was used to simulate the availability of oxygen during oil removal in the continuous annealing process; oxygen is available in the furnace gas atmosphere, in the form of iron oxides in contact with the rolling oil film on the steel surface and via the partial oxidation of the rolling oil film during cold rolling and coil storage (confirmed by infrared spectroscopic analysis of neat rolling oil and oily residue

extracted from the surface of cold rolled steel strip, results not shown). Rolling oils/oil ingredients were also analysed under high purity HNX to eliminate oxidation reactions and assess a viable alternative furnace cleaning atmosphere.

Samples were weighed into standard aluminium pans, placed onto platinum crucibles and loaded onto the TGA balance for analysis. A small amount of sample ( $1 \pm 0.1$  mg) was used to ensure maximum exposure of the oil to the aluminium surface and to the surrounding gas atmosphere. Data were analysed using Universal Analysis 2000 v3.3B software (TA Instruments).

#### **2.4.2 Pressure Differential Scanning Calorimetry (PDSC)**

Differential Scanning Calorimetry (DSC) is a thermal analysis technique that is commonly used to analyse material characteristics such as melting, crystallisation, glass transition, curing and chemical reactions.<sup>22</sup> There are two main types of DSC instruments; heat flux and power compensation. This review will only cover heat flux DSC as this is the type of instrument employed in this research.

A typical heat flux DSC cell comprises of a constantan disc that transfers heat to two pans, one containing the sample of interest and the other used as a reference (figure 2.5.).<sup>22</sup>

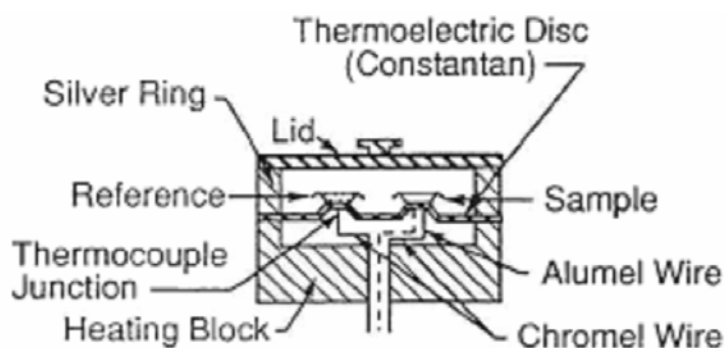


**Figure 2.5 Schematic diagram of a heat flux DSC cell.**<sup>22</sup>

The pans are maintained under a controlled gas environment (the gas type and flow rate are controllable) and subjected to a user-specified heating and/or cooling profile, which can include temperature ramps and/or isothermal conditions. Thermocouples placed in good thermal contact with the sample and reference pans measure a temperature difference which is converted to heat flow using calibration data. The resultant heat flow signal may then be plotted as a function of time or temperature, with changes in heat flow corresponding to either the adsorption (endothermic) or release (exothermic) of heat by the sample as compared to the reference, which in turn indicate the occurrence of physical or chemical changes. Endothermic responses are conventionally represented as negative.

One of the main limitations of DSC instruments is that they cannot be used to analyse volatile samples or samples that thermally decompose over the temperature range of interest. The loss of sample material during a DSC experiment typically interferes with measurements and causes noise in the output signal. It can also cause serious damage to the DSC cell, particularly if corrosive vapours are evolved.

Several variations of the standard DSC technique aim to accommodate the requirements associated with volatile sample analysis. Hermetic DSC pans, which can withstand the higher internal pressures caused by sample vapourisation, can be used in place of conventional DSC pans. However, hermetic pans preclude the sample from coming into contact with the surrounding gas atmosphere. This limits the application of hermetic pans and renders them a poor choice for the analysis of sample oxidation. The Sealed Capsule DSC (SCDSC) technique only partially rectifies this problem (refer to Chapter 1) as chemical reactions are restricted by the amount of gas in the sealed pan.<sup>26</sup> In order to overcome this limitation, a new DSC technique emerged in the 1960's that enabled experiments to be performed under high-pressure conditions (up to 7 MPa), thus eliminating sample evaporation.<sup>27</sup> This technique was dubbed 'Pressure Differential Scanning Calorimetry', or PDSC. PDSC has since been employed to study vapour pressure,<sup>28</sup> vapourisation kinetics,<sup>29</sup> polymer oxidative stability<sup>30</sup> and the pressure-dependence of polymer phase transitions.<sup>31-34</sup> However, as described in Chapter 1.2.2.2,

the most prevalent use of the PDSC technique has been in the lubricant industry to evaluate oxidative stability.<sup>15, 35-41</sup>

In the present work, DSC 2920 (TA Instruments) fitted with a high pressure cell was used for all PDSC analyses. Constant-volume conditions and an oxygen pressure of 3792 kPa (550 psi) were used to reduce oil volatilisation, maximise oxygen concentration and favour residue-forming reactions. The instrumental cell constant and temperature calibration were performed using indium. Rolling oil/oil ingredient samples were analysed in triplicate under continuous heating conditions ( $10\text{ }^{\circ}\text{C min}^{-1}$ ) between room temperature and  $500\text{ }^{\circ}\text{C}$ .  $1 \pm 0.1\text{ mg}$  of sample was weighed into a standard aluminium pan and placed onto the PDSC cell platform. The cell was then purged for  $\sim 30$  secs to establish an oxygen atmosphere before being sealed and pressurised. Data were analysed using Universal Analysis 2000 v3.3B software (TA Instruments).

### **2.4.3     ATR**

ATR spectra were obtained using a Nicolet Nexus 8700 FT-IR Spectrophotometer (Thermo Electron Corporation) fitted with a ‘Smart Orbit’ ATR accessory containing a diamond crystal internal reflection element. A background spectrum of an empty aluminium pan was acquired and subtracted from each sample spectrum. Spectral processing and analysis was performed using OMNIC version 7.1 software (Thermo Electron Corporation). All spectra were converted into absorbance units using the ‘ATR correct’ function. Baseline correction was performed where necessary using the ‘automatic baseline’ function.

#### **2.4.3.1   Mid-Infrared ATR**

The optimised collection parameters used for mid-infrared analysis of samples are summarised in table 2.5.

**Table 2.5 Summary of spectral collection parameters used in mid-infrared ATR experiments.**

<b>Parameter</b>	<b>Description</b>
Spectral range	4000-500 $\text{cm}^{-1}$
Number of scans	64
Resolution	4 $\text{cm}^{-1}$
Detector	DTGS TEC
Beamsplitter	KBr
Mirror velocity	0.6329 $\text{cm s}^{-1}$

### 2.4.3.2 Far-Infrared ATR

The optimised collection parameters used are summarised in table 4.6. The spectral range was selected due to the limitations of the diamond crystal internal reflection element; data acquired below 400  $\text{cm}^{-1}$  had a sawtooth appearance such that the lower limit for collection was set at 400  $\text{cm}^{-1}$ . The number of scans collected was greater than that used in mid-infrared analysis to improve the signal-to-noise ratio and a higher resolution was used to resolve overlapping bands. All spectra were converted into absorbance units using the 'ATR correct' function and smoothed using the 'automatic smooth' function to eliminate spectral noise.

**Table 4.6 Summary of spectral collection parameters used in far-infrared ATR experiments.**

<b>Parameter</b>	<b>Description</b>
Spectral range	600-400 $\text{cm}^{-1}$
Number of scans	256
Resolution	2 $\text{cm}^{-1}$
Detector	DTGS PE
Beamsplitter	Solid Substrate
Mirror velocity	0.6329 $\text{cm s}^{-1}$

## 2.4.4 Hot Dip Simulation

### 2.4.4.1 Optical Microscopy

Characterisation of hot dip simulation sample coating quality was achieved by optical microscopy. The top 40 mm on the best-coated side of each sample was analysed (figure 2.6).

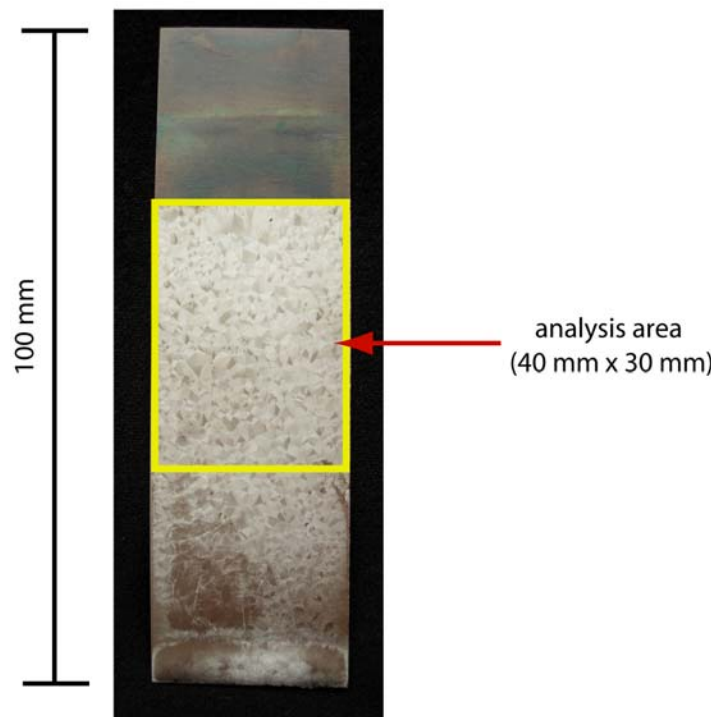


**Figure 2.6** Typical hot dip simulation sample for which the area of analysis is indicated.

The imaging apparatus (figure 2.7) consisted of a Panasonic GP-KR222E CCD camera fitted with an Olympus 3.2 x magnification lens, an illuminated sample stage and a PC equipped with a frame-grabber card. Images were acquired and analysed using Video Pro 32 (v 4.070, 1999) software. Calibration of the software for surface area measurement was achieved by imaging and measuring the surface area of a square of known dimensions. The surface area occupied by uncoated defects ( $A_{\text{uncoated}}$ , the area of the imaged surface below a set contrast threshold) was then determined and ratioed

against the total surface area ( $A_{total}$ ) according to equation 2.3 to determine the % uncoated defect area for each sample:

$$\% \text{ Uncoated Defect Area} = \frac{A_{uncoated}}{A_{total}} \times 100 \quad \text{Equation 2.3}$$

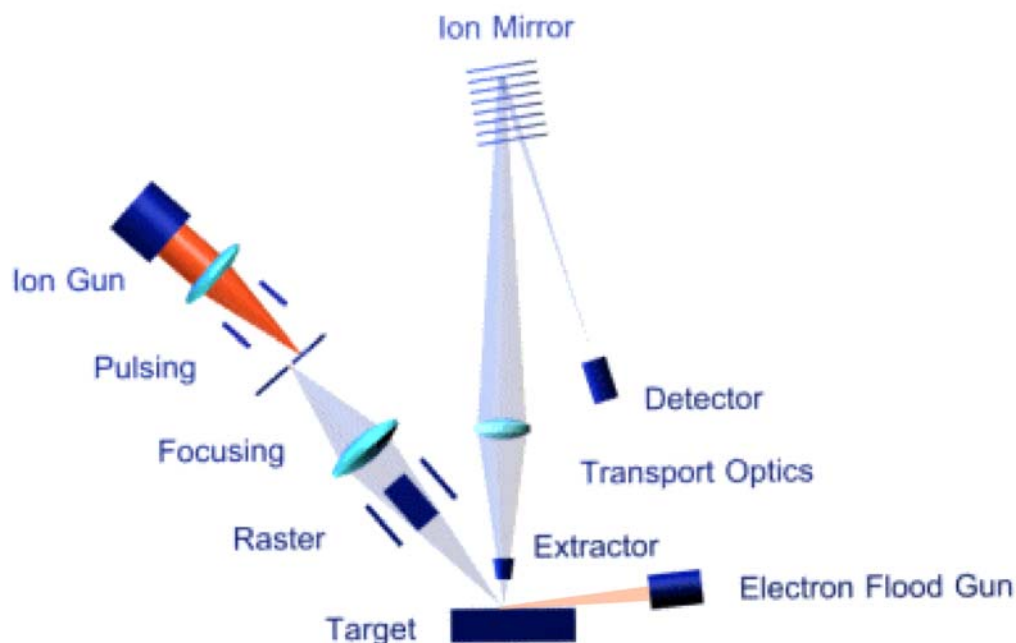
The % uncoated defect area values reported are the average of measurements made on two hot dipped samples.



Figure 2.7 Imaging apparatus used to analyse hot dip simulation samples.

#### 2.4.4.2 Time-of-Flight Secondary Ion Mass Spectrometry (ToF-SIMS)

ToF-SIMS is a sensitive technique for characterising the chemical composition of surfaces. A ToF-SIMS instrument typically comprises of an ultrahigh vacuum system, a primary ion gun, a flight path and a mass detector system (figure 2.8).



**Figure 2.8 Schematic diagram of a ToF-SIMS instrument.**<sup>42</sup>

The sample of interest is bombarded with a pulsed beam of primary ions, which can interact with atoms within the outer few layers of the surface via a series of collisions (figure 2.9).<sup>43, 44</sup> Atoms and/or molecules within these layers may receive sufficient energy from these collisions to be ejected from the surface and into the vacuum. Although the ejected species may be in a neutral, excited or ionised state, only ionised species of a particular charge (positive or negative secondary ions) are analysed. The secondary ions are extracted into the ToF column and an accelerator grid is used to adjust the velocity of the ions such that they have the same initial kinetic energy. Charged steering plates are used to collimate the secondary ions and ensure that they are travelling in the appropriate direction to hit the secondary ion detector. Since the ions all have the same kinetic energy, the lighter ions travel faster such that a mass spectrum is constructed by ions of different masses hitting the detector at different times. This technique may be combined with sputtering of successive surface layers using a second ion beam to create a profile of secondary ions detected at different depths within the surface (depth profiling).<sup>45</sup>

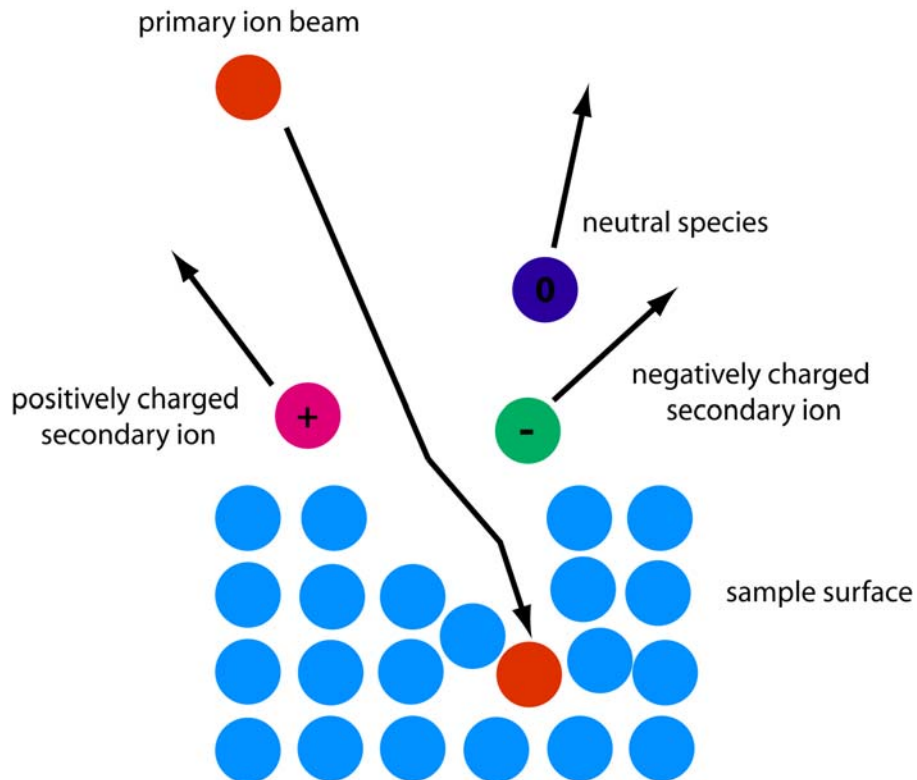


**Figure 2.9** Schematic diagram showing primary ion interactions with the sample surface.

ToF-SIMS measurements were performed by Dr Grant van Riessen at the Centre for Materials and Surface Science at LaTrobe University using a ToF-SIMS IV instrument (Ion-ToF GmbH, Germany). Spectra were acquired within uncoated areas, or just above the alloy coating where no uncoated areas were present, on three representative 55Al-43.4Zn-1.6Si hot dip simulation coated samples prepared from an untreated steel control and from steel treated with neat DAPS and SLO respectively. A  $\text{Cs}^+$  ion beam was used to sputter over a  $300 \mu\text{m}^2$  area of the surface and a  $\text{Bi}^+$  primary ion beam was then used to create negatively charged secondary ions, which were collected over a  $100 \mu\text{m}^2$  region within the  $300 \mu\text{m}^2$  sputtered area. Charge neutralisation was achieved using a pulsed electron flood gun. Spectra were acquired in the mass range 1-600 atomic mass units (amu). The ion intensities reported in depth profile spectra (the intensity of ion  $x$  at time  $t$ ,  $I(x)_t$ ) are ratioed against the intensity of the  $^{56}\text{Fe}$  ion at time  $t$ ,  $I(^{56}\text{Fe})_t$ , and

normalised against the initial ion intensity,  $I(x)_{t=0}$ , to enable a semi-quantitative comparison between the samples (equation 2.4).

$$\frac{I(x)_t}{I(^{56}\text{Fe})_t} / I(x)_{t=0} \quad \text{Equation 2.4}$$

## **2.4.5 Industrial-Scale Hot Dipping Trials**

The industrial hot dipped samples were characterised by visual inspection, optical microscopy and Scanning Electron Microscopy (SEM) as outlined below.

### **2.4.5.1 Visual Inspection**

Visual inspection of industrial hot dipped samples was performed to enable classification of the resultant metallic coating quality as being defect-free (no visible uncoated defects) or containing pinhole uncoated (tens of microns in dimension), fine to medium uncoated (hundreds of microns to millimetre size range) or gross uncoated (millimetres to centimetres in dimension) defects. Photographs of industrial hot dipped samples were acquired using a Nikon Coolpix 4200 camera.

### **2.4.5.2 Optical Microscopy**

Optical microscopy analysis of the industrial hot dipped samples was performed using a Leica DMRM Microscope operating in bright-field reflectance mode using lenses at a magnification ranging between 100-500 x. Samples were observed in real time using a computer connected to a Panasonic GP-KR222E CCD camera and images were acquired using a frame-grabber card and analysed with Video Pro 32 (v 4.070, 1999) software.

### **2.4.5.3 Scanning Electron Microscopy (SEM)**

SEM is common technique for the analysis of surface structure and elemental composition and has been used extensively in the characterisation of metallic and

organo-polymeric coating defects.<sup>18, 46, 47</sup> SEM differs from optical microscopy as it employs an electron beam, as opposed to visible light, as the radiation source. Since electrons have a significantly shorter wavelength than light photons, much greater resolution can be achieved in SEM imaging than in standard optical microscopy.<sup>46</sup> This ensures that samples can be imaged at much higher magnification without a concomitant loss in detail; surface features on the nanometre-scale may be spatially resolved using field-emission SEM.<sup>18</sup> The principles of the SEM technique are shown in figure 2.10.

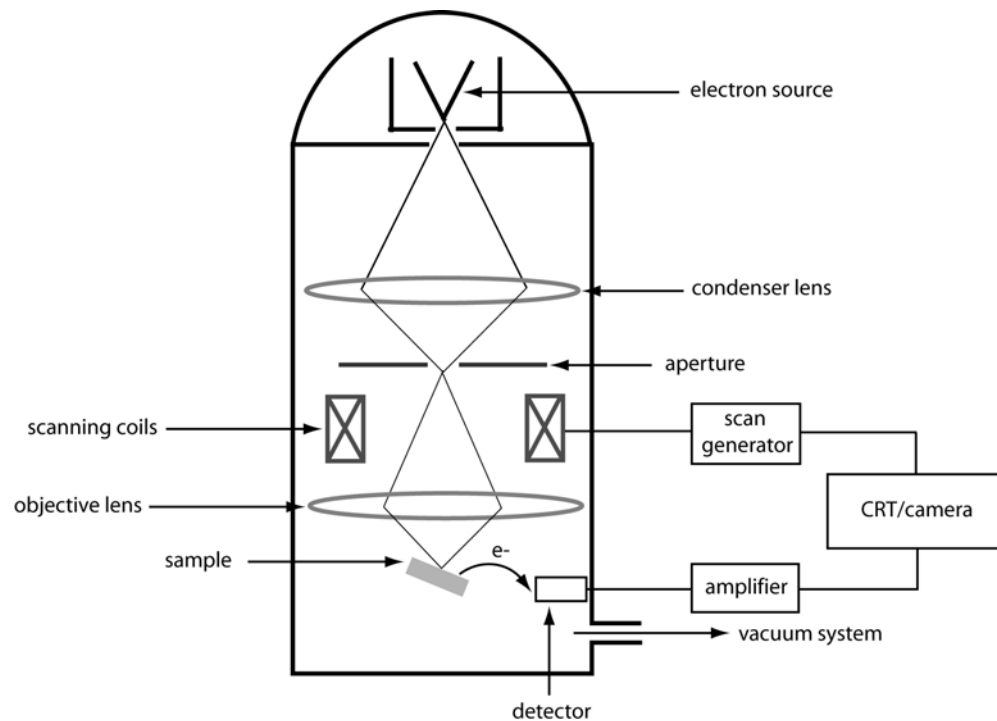


**Figure 2.10 Schematic diagram of a Scanning Electron Microscope.**

Electrons from the emission source or filament are accelerated by a voltage typically in the range 1-30 kV and directed down the centre of a column containing several lenses. These lenses condense and focus the electron beam, which is subsequently deflected back and forth across the sample surface by a magnetic field created by scan coils. Interactions between the incident (primary) electrons and atoms beneath the sample surface result in various phenomena (figure 2.11) including the ejection of secondary

electrons. The secondary electrons strike a secondary electron detector and the resulting current is amplified and used to modulate the brightness of a cathode ray tube (CRT) to progressively construct an image corresponding to sample topography. Analysis of X-rays emitted from the sample (Energy Dispersive Spectroscopy, or EDS) can provide semi-quantitative information on elemental composition.

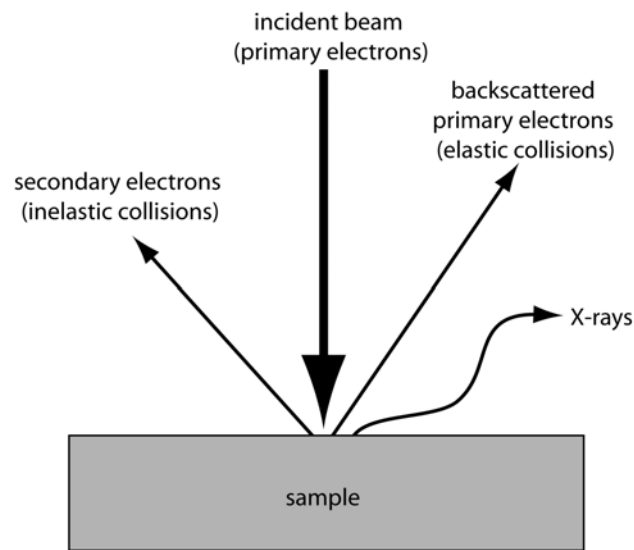


**Figure 2.11 Key interactions between primary electrons and the sample surface during SEM.**

SEM analysis of industrial hot dipped samples was undertaken at Adelaide Microscopy using a Philips XL20 Scanning Electron Microscope. The samples were sufficiently conductive and did not require sputter coating. A 15 kV primary electron beam was used for imaging with the detection of emitted electrons using a secondary electron detector. Analysis of emitted X-rays was achieved using an EDAX DX4 detector.

#### **2.4.6 High Temperature Laser Scanning Confocal Microscopy (LSCM)**

LSCM is an imaging technique used extensively in the analysis of biological samples and, more recently, for high temperature metallurgical studies.<sup>48</sup> It offers several

advantages over conventional light microscopy, including the reduction or elimination of out-of-focal-plane information and the ability to control depth of field.<sup>48, 49</sup> The confocal principle is illustrated in figure 2.12.<sup>50</sup> A 632.8 nm He-Ne laser beam is passed through a beam splitter and focused onto the sample surface using an objective lens. Reflected light then passes back to a detector which is screened by a pinhole aperture. The aperture excludes light originating from positions other than the focal point such that a clear, intense signal from the focal point is obtained. An image of the sample surface is then constructed by scanning the sample surface at various focal points in real time.

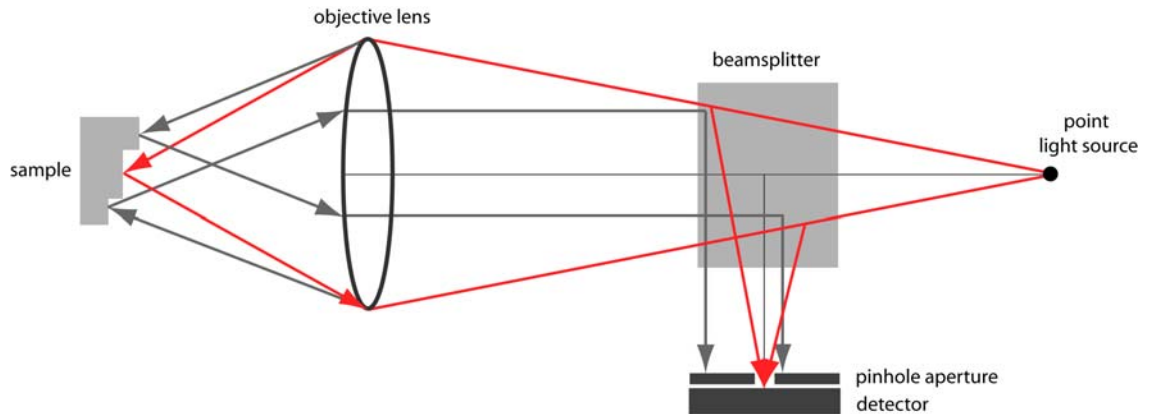


**Figure 2.12 Schematic diagram showing the principle of confocal optics.<sup>50</sup>**

The apparatus used in the present research consists of a LSCM attached to a gold-plated ellipsoid infrared heating furnace (figure 2.13).<sup>51</sup> Assistance in carrying out LSCM experiments was provided by Mr Mark Reid. The sample assembly, located at one focal point of the cavity, is heated by a halogen lamp located at the second focal point. A quartz plate is used to separate the sample and lamp chambers so that the atmosphere within the sample chamber can be controlled.

6.3 mm<sup>2</sup> cold rolled steel samples were cut and cleaned by rinsing in acetone followed by ethanol (the samples were not pickled in HCl solution due to their small size). A thin

film of rolling oil was subsequently placed on the sample surface using a cotton bud applicator.

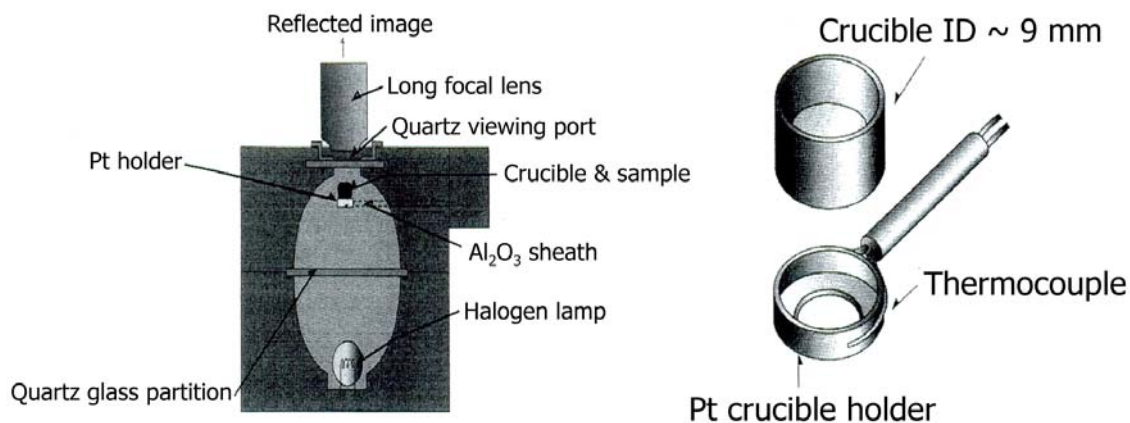


**Figure 2.13 Schematic diagram of the laser scanning confocal microscope furnace and sample holder.<sup>51</sup>**

The sample was then placed into a ~ 9 mm inner-diameter alumina crucible and loaded onto the crucible holder (refer to figure 2.13) and into the infrared heating furnace. The furnace was left at atmospheric pressure under the laboratory air atmosphere (as opposed to being purged with an inert argon atmosphere) to provide a source of oxygen enabling rolling oil thermo-oxidative decomposition. A heating rate of  $100\text{ }^{\circ}\text{C min}^{-1}$  was then applied to heat the sample from room temperature to  $600\text{ }^{\circ}\text{C}$ . The temperature of the sample, measured by thermocouples incorporated into the sample holder, was recorded simultaneously with the sample image on a DVD at a rate of 30 frames per second. Still images were then obtained using image analysis software. Analyses were performed in duplicate and solvent-cleaned, untreated steel was analysed as a control.

## 2.5 Error Analysis

Errors are reported as the coefficient of variation (percent relative standard deviation) determined according to equation 2.5:<sup>52</sup>

$$CV = \left( \frac{s}{\bar{x}} \right) \times 100\% \quad \text{Equation 2.5}$$

where CV is the coefficient of variation, s is the standard deviation and  $\bar{x}$  is the mean. For data sets (such as the TGA data in table 3.1), the maximum error margin is quoted.

## 2.6 References

1. Gibson, A., Pers. Comm. In 2003.
2. Sech, J. M., Oleksiak, T. P., *Iron Steel Eng.* **1995**, 72, 33.
3. Pilon, A. C., Cole, K. C., Noel, D. In *Surface characterization of cold-rolled steel by grazing-angle reflection-absorption FT-IR spectroscopy*, SPIE Proc. - 7th Int. Conf. on Fourier Transform Spectrosc., 1989, pp 209.
4. Shamaingar, M., *Iron Steel Eng.* **1967**, 44, 135.
5. Keyser, A. G., Kunkel, K. F., Snedaker, L. A., *Iron Steel Eng.* **1998**, 75, 43.
6. Svedung, D. H., *Scand. J. Metall.* **1980**, 9, 183.
7. Lafargue, P. E., Chaoui, N., Millon, E., Muller, J. F., Derule, H., Popandec, A., *Surf. Coat. Technol.* **1998**, 106, 268.
8. Chen, F., Patil, R. In *An in-depth analysis of various subtle coating defects of the 2000's*, Galvatech '04 - Proc. 6th Int. Conf. on Zinc and Zinc Alloy Coated Steel Sheet, Chicago, USA; 2004, pp 1055.
9. Tang, N.-Y., Goodwin, F. E. In *A study of defects in galvanized coatings*, Galvatech '01 - Proc. 5th Int. Conf. on Zinc and Zinc Alloy Coated Steel Sheet, Brussels, Belgium; 2001, pp 49.
10. Willem, J.-F., Claessens, S., Cornil, H., Fiorucci, M., Hennion, A., Xhoffer, C. In *Solidification mechanisms of aluzinc coatings - effect on spangle size*, Galvatech '01 - Proc. 5th Int. Conf. on Zinc and Zinc Alloy Coated Steel Sheet, Brussels, Belgium; 2001, pp 401.
11. Puente, J. M., Alonso, F. J., Andres, L., Prado, M. In *Influence of an adequate surface conditioning on the final characteristics of GI for exposed panels use on*

*automotive sector*, Galvatech '04 - Proc. 6th Int. Conf. on Zinc and Zinc Alloy Coated Steel Sheet, Chicago, USA; 2004, pp 457.

12. Zhang, Y., Pei, P., Perez, J. M., Hsu, S. M., *Lubr. Eng.* **1992**, 48, 189.
13. Zhang, Y., Perez, J. M., Pei, P., Hsu, S. M., *Lubr. Eng.* **1992**, 48, 221.
14. Evans, R., Frelin, J., Morrison, S., *Measurement of the oxidative polymerisation properties of rolling oil lubricants using the PDSC technique, and its relationship to Zinalume coating compatibility at BHP Steel Port Kembla*; Quaker Chemical Corporation Corporate Technology Laboratory: 6th November, 1998; pp 1.
15. Sharma, B. K., Stipanovic, A. J., *Thermochim. Acta* **2003**, 402, 1.
16. Abou El Naga, H. H., Salem, A. E. M., *Wear* **1984**, 96, 267.
17. Crews, P., Rodriguez, J., Jaspars, M., *Organic Structure Analysis*. Oxford University Press: New York, USA, 1998.
18. Walzak, M. J., Davidson, R., Biesinger, M., *J. Mater. Eng. Perf.* **1998**, 7, 317.
19. Niu, B. J., Urban, M. W., *J. Appl. Polym. Sci.* **1998**, 70, 1321.
20. Almeida, E., Balmayore, M., Santos, T., *Prog. Org. Coat.* **2002**, 44, 233.
21. Williams, J. Surface reactions of zinc vapour with steel relevant to the Zn-55%Al-1.5%Si hot dip metal coating process. University of Wollongong, Wollongong, 2005.
22. Gallagher, P. K., Thermoanalytical Instrumentation, Techniques, and Methodology. In *Thermal Characterization of Polymeric Materials, 2nd edition*, Turi, E. A., 'Ed.'; Academic Press, Inc.: New York, USA, 1997; 'Vol.' 1.
23. Blaine, R., *Am. Lab.* **1998**, 30, 21.
24. Blaine, R. L., Hahn, B. K., *J. Therm. Anal. Cal.* **1998**, 54, 695.
25. Blaine, R. L. Method and apparatus of modulated-temperature thermogravimetry. US 6113261, 2000.
26. Bowman, W. F., Stachowiak, G. W., *Tribol. Int.* **1996**, 29, 27.
27. Shamis, S., Pers. Comm. In 2003.
28. Casserino, M., Blevins, D. R., Sanders, R. N., *Thermochim. Acta* **1996**, 284, 145.
29. Rao, S. P., Pai, V., Surianarayanan, M., Mallikarjunan, M. M., *Thermochim. Acta* **1996**, 279, 157.

30. Riga, A., Collins, R., Mlackak, G., *Thermochim. Acta* **1998**, 324, 135.
31. Vanden Eynde, S., Mathot, V. B. F., Hohne, G. W. H., Schawe, J. W. K., Reynaers, H., *Polymer* **2000**, 41, 3411.
32. Hohne, G. W. H., *Thermochim. Acta* **1999**, 332, 115.
33. Rastogi, S., Hohne, G. W. H., Keller, A., *Macromolecules* **1999**, 32, 8897.
34. Hohne, G. W. H., Rastogi, S., Wunderlich, B., *Polymer* **2000**, 41, 8869.
35. Rhee, I.-S. In *Development of a new oxidation stability test method for greases using a pressure differential scanning calorimeter*, NLGI 27th Annual Meeting, Denver, USA; 1990, pp 1.
36. Senthivel, P., Joseph, M., Nagar, S. C., Anoop, K., Naithani, K. P., Mehta, A. K., Raje, N. R., *NLGI Spokesman* **2005**, 69, 26.
37. Rhee, I.-S., *NLGI Spokesman* **2001**, 65, 16.
38. Zeman, A., Stuwe, R., Koch, K., *Thermochim. Acta* **1984**, 80, 1.
39. Kauffman, R. E., Rhine, W. E., *Lubr. Eng.* **1988**, 44, 154.
40. Adamczewska, J. Z., Love, C., *J. Therm. Anal. Cal.* **2005**, 80, 753.
41. Gamlin, C. D., Dutta, N. K., Choudhury, N. R., Kehoe, D., Matisons, J., *Thermochim. Acta* **2002**, 392-393, 357.
42. Ion-ToF Time of Flight Mass Spectrometer. <http://www.iontofusa.com/tof.htm> (21/09/2007).
43. Sykes, D. E., Dynamic Secondary Ion Mass Spectroscopy. In *Methods of Surface Analysis*, Walls, J. M., 'Ed.'; Cambridge University Press: Cambridge, UK, 1989; pp 216.
44. MacDonald, R. J., King, B. V., SIMS - Secondary Ion Mass Spectrometry. In *Surface Analysis Methods in Materials Science*, O'Connor, D. J., Sexton, B. A., Smart, R. St. C., 'Ed.'; Springer-Verlag: New York, USA, 1992; 'Vol.' 23, pp 117.
45. King, B. V., Sputter Depth Profiling. In *Surface Analysis Methods in Materials Science*, O'Connor, D. J., Sexton, B. A., Smart, R. St. C., 'Ed.'; Springer-Verlag: New York, USA, 1992; 'Vol.' 23, pp 97.

46. Dann, S. E., *Reactions and Characterization of Solids*. The Royal Society of Chemistry: Cambridge, UK, 2000.
47. Payling, R., Coated Steel. In *Surface Analysis Methods in Materials Science*, O'Connor, D. J., Sexton, B. A., Smart, R. St. C., 'Ed.'; Springer-Verlag: New York, USA, 1992; 'Vol.' 23, pp 387.
48. Sridhar, S. In *Application of confocal laser microscopy to steel research*, ICS 2005, Charlotte, North Carolina, USA; 2005, pp 797.
49. Claxton, N. S., Fellers, T. J., Davidson, M. W. Laser scanning confocal microscopy. [www.olympusconfocal.com/theory/LSCMIntro.pdf](http://www.olympusconfocal.com/theory/LSCMIntro.pdf) (17/09/07).
50. Phelan, D., High temperature confocal scanning laser microscope operating instructions. In; University of Wollongong: 2002; pp 1.
51. Phelan, D., Reid, M., Dippenaar, R., *Metall. Mater. Trans. A* **2006**, 37A, 985.
52. Skoog, D. A., West, D. M., Holler, F. J., *Fundamentals of Analytical Chemistry, 5th edition*. Saunders College Publishing: Philadelphia, USA, 1996.